A Combinatorial Approach for Directing the Amount of Fibronectin Fibrils Assembled by Cells that Uses Surfaces Derivatized with Mixtures of Fibronectin and Cell Binding Domains

Pradnya P. Kshatriya
Dept. of Chemical and Biological Engineering, Illinois Institute of Technology, Chicago, IL 60616

Stella W. Karuri
Biometrics Research Branch, National Cancer Institutes, Bethesda, MD 20952

Chunyi Chiang and Nancy W. Karuri
Dept. of Chemical and Biological Engineering, Illinois Institute of Technology, Chicago, IL 60616

DOI 10.1002/btpr.1537
Published online May 21, 2012 in Wiley Online Library (wileyonlinelibrary.com).

Fibrillar fibronectin (FN) has the crucial role of attracting and attaching cells as well as molecules that mediate tissue repair during wound healing. A previous study demonstrated higher extracellular staining of FN fibrils in cells cultured on surfaces tethered with an equimolar mixture of a FN binding domain and FN's cell binding domain, III_{1-2} and III_{9-10} respectively, than on surfaces with III_{9-10} alone. The effect of varying surface amounts of III_{1-2} and III_{9-10} on the quantity of FN fibrils formed by NIH-3T3 fibroblasts was examined. GST tagged III_{1-2} and III_{9-10} were conjugated to polyurethane surfaces and ELISAs were used to identify the experimental design space or the range of concentrations of GST-III_{1-2} and GST-III_{9-10} that demarcated the limits of protein loading on the surface. When GST-III_{1-2} was fixed and GST-III_{9-10} varied within the design space, the amount of FN fibrils measured by immunoblotting detergent insoluble cell lysates was dependent on the ratio of III_{9-10} to III_{1-2}. When the total protein concentration was fixed and the mixture composition of GST-III_{1-2} and GST-III_{9-10} varied such that it optimally covered the design space, a parabolic relationship between FN fibril amount and the ratio of III_{9-10} to III_{1-2} was obtained. This relationship had a maximum value when the surface was bonded to equal amounts of III_{1-2} and III_{9-10} ($P < 0.05$). Thus the ratio of III_{9-10} to III_{1-2} can be utilized to direct the quantity of FN fibrils formed on surfaces. © 2012 American Institute of Chemical Engineers *Biotechnol. Prog.*, 28: 862–871, 2012
Keywords: fibronectin, cell binding domain, fibronectin binding domain, fibronectin fibril, extracellular matrix

Introduction

Skin tissue is held together by a cellular scaffold or extracellular matrix (ECM) that is important for homeostasis. This ECM is assembled by cells from secreted fibronectin (FN), collagen Types I, III, and VI as well as proteoglycans.[1,2] In the event of an injury, fibrillar FN plays the critical role of recruiting and binding cells and molecules that lead to tissue and ECM repair.[3] A deficiency in fibrillar FN in chronic wounds has been linked to impaired healing and may be due to proteolysis of FN by molecules produced by immune cells.[4–6] The products of proteolysis stimulate the immune system further and increase the degradative atmosphere. Current treatments for chronic wounds rely on decellularized ECMs.[6] However, the chemical treatments used to harvest these ECMs may retard their activity in wound healing. Synthetic materials that accelerate the assembly of FN into fibrils may reduce soluble FN available for proteolytic degradation and reset the healing clock in chronic wounds.

FN is a dimeric protein composed of multiple functional domains that bind cells, through transmembrane intergrin receptors.[7] It also binds ECM components and other FN molecules.[7] FN fibril formation is initiated when cells bind to the cell-binding domain in the ninth and tenth Type III repeats, III_{9-10}, through interactions with $\alpha_5\beta_1$ integrins.[8,9] Cell spreading leads to conformational changes in attached FN[10] that are thought to expose cryptic FN-FN binding sites. Native and cryptic FN binding sites have been identified in the first two Type III repeats, III_{1-2}.[11,12] III_{1-2} is important for FN fibril formation because cells cultured with recombinant FN that is missing III_{1-2} are unable to form FN fibrils.[9] Furthermore, antibodies against III_{1-2} inhibit FN fibril formation.[13,14] FN fragments have been used extensively to map

Additional Supporting Information may be found in the online version of this article.

Correspondence concerning this article should be addressed to N. W. Karuri at nkaruri1@iit.edu.

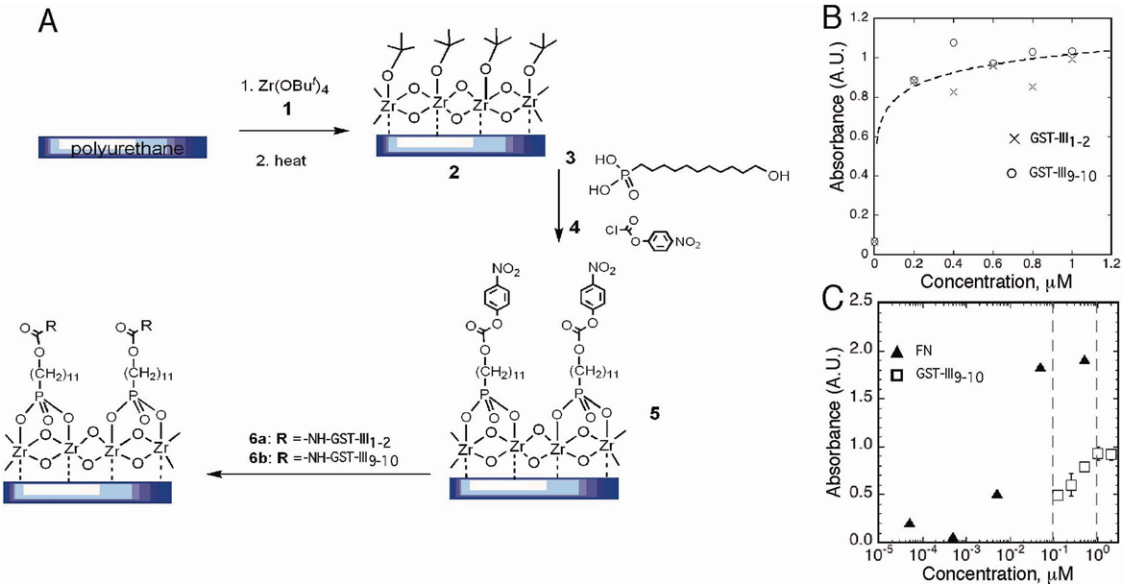

Figure 1. Derivatizing and characterizing polyurethane surfaces with GST-III$_{1-2}$ and GST-III$_{9-10}$.

A: Polyurethane surfaces were functionalized using the method of[15] by reacting with zirconium *tert*-butoxide (1) to form a layer of zirconium oxide (2). This was reacted with phosphonic acid (3) and nitrophenyl chloroformate (4) to form the activated surface (5). GST-III$_{1-2}$ and GST-III$_{9-10}$ (6) were then attached to the functionalized surfaces through coupling lysine residues with the surface carbonate. B: Bound GST-III$_{1-2}$ and GST-III$_{9-10}$ at different solution concentrations were detected using ELISAs with polyclonal R184 and monoclonal 7.1 antibodies specific to III$_{1-2}$ and III$_{9-10}$, respectively. The broken line is a fit of III$_{1-2}$ and III$_{9-10}$ ELISA absorbances. C: Control ELISA study of FN and GST-III$_{9-10}$ on activated surfaces detected with 7.1 antibodies. Solution concentrations corresponding to surface saturation are marked by the broken lines. [Color figure can be viewed in the online issue, which is available at wileyonlinelibrary.com.]

sites that are important for FN fibrillogenesis[7] but there are no published studies on how synthetic materials can be used to direct FN fibril formation.

We recently reported that fibroblasts cultured on nonfouling polyurethane surfaces derivatized with equal amounts of III$_{1-2}$ and III$_{9-10}$ had higher staining intensity of FN fibrils than fibroblasts cultured on surfaces with III$_{9-10}$ alone.[15] This work provides a continuum to our previous study by investigating the influence of surfaces derivatized with different amounts of III$_{1-2}$ and III$_{9-10}$ on FN fibril formation by fibroblasts. The key to understanding the relationship between different surface amounts of III$_{1-2}$ and III$_{9-10}$, and cellular responses is the judicious choice of levels of experimental factors during experimental design. We have determined a design space marked by the limits of protein loading on the surface and used two experimental approaches to examine the influence of varying amounts of glutathione *S*-transferase (GST) tagged III$_{1-2}$ and III$_{9-10}$, in the design space, on FN fibril formation. In the first design, the concentrations of GST-III$_{1-2}$ were fixed and the concentrations of GST-III$_{9-10}$ were varied over the experimental range. This approach allowed us to identify that the ratio of III$_{9-10}$ to III$_{1-2}$ correlated to FN fibril amount. In the second design approach, we used a statistical approach to optimally sample GST-III$_{1-2}$ and GST-III$_{9-10}$ concentrations within the design space. Maximum coverage of the design space established that FN fibril amount is dependent on the ratio of III$_{9-10}$ to III$_{1-2}$ and has a maximum when the ratio of III$_{9-10}$ to III$_{1-2}$ is one. The biological responses of cell spreading and FN fibril amount fit well-defined mathematical relationships but follow different trends with the ratio of III$_{9-10}$ to III$_{1-2}$. Thus, the ratio of III$_{9-10}$ to III$_{1-2}$ can be used to engineer instructive biomaterials for FN fibril formation as therapeutics for chronic wounds.

Materials and Methods

Substrate preparation and characterization

Polyurethane substrates were prepared and characterized as described in Ref. 15. Polyurethane surfaces were first activated for peptide binding by reaction with zirconium tetra(-*tert*-butoxide) vapor (Sigma-Aldrich, St. Louis, MO) which is compound 1 in Figure 1A. This results in a metal oxide layer on the surface of polyurethane (Surface 2, Figure 1A). The metal oxide was sequentially reacted with phosphonic acid (a kind gift from Jeffrey Schwartz, Princeton University) and *p*-nitrophenyl chloroformate (Sigma-Aldrich): molecules 3 and 4, respectively, in Figure 1. Phosphonic acid conjugation was carried out by suspending the polyurethane substrates in 0.1 mM of phosphonic acid in absolute ethanol and allowing the solution to evaporate at ambient temperature. After which, chloroformate coupling was carried out by immersing the substrates in 1 mg/mL of the *p*-nitro phenyl chloroformate in diethyl ether in a moisture free environment. A dry environment is essential in this step to avoid the spontaneous hydrolysis of phenyl chloroformate by water. Changes in surface chemistry were monitored by contact angle measurements. The contact angle is the angle which the water–air interface makes with the solid surface. Changes in surface chemistry are often accompanied by changes in the wetting properties of a surface and subsequently changes in contact angle.[16] Contact angles near zero indicate good wetting and a hydrophilic surface, whereas contact angles greater than 90° indicate poor wetting and a hydrophobic surface. The contact angles were measured in a contact angle meter (ChemInstruments, Mentor, OH).

After chloroformate treatment, the substrates were immersed in phosphate-buffered saline at pH 8 containing

the protein solutions and incubated for 1 h at room temperature. The surfaces were passivated with 100 mM Tris-HCl at pH 8. The protein solutions consisted of GST fusions of FN domains: GST-III_{1-2} and GST-III_{9-10}. The GST recombinant proteins were purified from a bacterial expression system as described in Refs. 15 and 17. The bacteria were a kind gift from Dr. Jean Schwarzbauer, Princeton University. Solution concentrations were varied from 0 to 4 μM in Dulbecco's phosphate-buffered salt solution (PBS, Mediatech, Manassas, VA). All the studies were conducted with the GST-fusion proteins.

Detection of FN domains by enzyme-linked immunosorbent assays

Enzyme-linked immunosorbent assays (ELISAs) were used to detect the amount of protein bound on the activated polyurethane surfaces. Functionalized polyurethane samples were placed in a 24-well plate and blocked with 1% bovine serum albumin (BSA) in PBS (Fisher Scientific, Pittsburg, PA) for 1 h at 37°C. The samples were then incubated with polyclonal R184 antibodies and monoclonal 7.1 antibodies (both a kind gift from Dr. Schwarzbauer) in 1% BSA in PBS. R184 and 7.1 bind III_{1-6} and III_{9-10}, respectively. After three washes with 1% BSA in PBS, the samples were incubated with biotinylated goat anti-mouse IgG, H+L (Pierce, Rockford, IL) or goat anti-rabbit IgG, H+L (Pierce) for 1 h at 4°C. The samples were washed, and then streptavidin, β-galactosidase conjugate (Invitrogen, Grand Island, NY), at 1:500 dilution in a 1% BSA in PBS solution containing 1.5 mM $MgCl_2$ and 2 mM β-mercaptoethanol (Sigma-Aldrich), was used to bind biotin. After washing the samples six times with 1% BSA in PBS, 1 mg/mL of *p*-nitrophenyl β-D-galacto-pyranoside (Sigma-Aldrich) was added and the samples were incubated for an hour at room temperature. During this period, the optical density at 405 nm was determined at 10-min time intervals using an ELx800 plate reader (BioTek Instruments, Winooski, VT). Negative controls consisted of the functionalized surfaces without GST-III_{1-2} or GST-III_{9-10}.

Experimental design

The design space or the range of experimental concentrations pertaining to the relevant GST-III_{1-2} and GST-III_{9-10} mixture concentrations was identified from ELISA data. The upper limit of the design space was marked by the saturation concentration of GST-III_{1-2} and GST-III_{9-10} on the surface, whereas the lower limit was zero. Two experimental designs were used. In the first design, GST-III_{1-2} concentration was fixed and GST-III_{9-10} varied. The total bulk mass concentration of the protein was kept constant and at surface saturation point by adding GST. In the second approach, a coverage design was used.[18] The coverage design generates possible GST-III_{1-2} and GST-III_{9-10} concentrations that optimally cover the design space. Such designs are a common feature in "black-box" experiments where the relationship between the outcome and the experimental factors is unknown.[19] The coverage design was implemented by the R package "fields,"[20] which helps to identify 24 points that are well spaced based on an averaged distance metric. Each point in the design consists of a pair of values, which identify mixture concentrations of GST-III_{1-2} and GST-III_{9-10}. We chose 24 points as these correspond to the number of samples that can be accommodated in a 24-well culture plate.

Cell preparation

Mouse embryonic fibroblasts, NIH 3T3 fibroblasts (ATCC, Manassas, VA) were grown to 80–90% confluence in 10 cm dishes at 35°C with 5% CO_2. Dulbecco's modified Eagle's medium (DMEM) supplemented with 10% bovine calf serum (BCS; Sigma-Aldrich, Co.) was used for maintaining the cells. Cells at passages 15–34 were used for the experiments. After achieving the desired confluence, the cells were washed in PBS and trypsinized using 1 mg/mL of TPCK trypsin (Fisher Scientific) in 0.01% ethylenediaminetetracetic acid (Fisher Scientific) for 5 min at room temperature. Trypsin was then inactivated by the addition of 0.5 mg/mL soybean trypsin inhibitor (Fisher Scientific) in PBS. The cells were isolated from the bulk solution in a pellet by centrifuging for 5 min at 1,000 rpm. This procedure was repeated twice to remove any residual trypsin. After the last spin, the cells were resuspended in DMEM without serum.

Cell adhesion assays

NIH 3T3 fibroblasts in serum-free DMEM were added to each sample in a 24-well culture plate. A cell density of 1×10^4 cells per well and a volume of 0.5 mL cells per well of serum-free DMEM was used. The samples were incubated at 37°C with 5% CO_2 for 1 h, and then washed twice with PBS. The adherent cells were fixed in 3.7% paraformaldehyde (Fisher Scientific) in PBS for 15 min at room temperature, and then permeabilized with 0.5% NP-40 detergent (Fisher Scientific) in PBS for 15 min at room temperature. The cells were washed twice with PBS and then labeled with Hoechst 33258 (Fischer-Scientific) and fluorescein phalloidin (Invitrogen) at concentrations of 1 μg/mL and a dilution of 1:50 in 2% ovalbumin, respectively (Fisher Scientific). The samples were incubated at 37°C for 30 min, washed with PBS three times, and finally rinsed once with water. The samples were then mounted onto glass slides using antifade media (Prolong antifade, Invitrogen) and imaged.

Development and characterization of FN fibrils in the ECM

Fibroblasts were plated on GST-III_{1-2} and GST-III_{9-10} functionalized surfaces at a density of 2×10^5 cells per well in DMEM without serum. The volume of DMEM used was 0.5 mL per well. After half an hour, the media was changed to DMEM supplemented with 10% BCS that had been depleted of FN and culture was maintained for 24 h. FN was depleted from BCS by affinity chromatography on a column with Gelatin Sepharose 4B beads (GE Healthcare, Piscataway, NJ) and was validated by sodium dodecyl sulfate polyacrylamide gel electrophoresis (SDS-PAGE) and immunoblotting analyses of the column flow through. FN fibrils in the ECM were characterized by immunofluorescence microscopy or by immunoblotting. Immunofluorescence staining of FN was carried out by washing the cells with PBS, fixing in paraformaldehyde, and labeling with R457 antibodies at a 1:200 dilution (a gift from Dr. Schwarzbauer) and fluorescein goat anti-rabbit IgG (H+L) antibodies (Invitrogen). Immunoblotting studies of FN are described below.

Immunoblotting of FN in deoxycholate detergent insoluble fractions

After 24 h of cell culture, the ECM was isolated by lysing the cells in 150 μL of lysis buffer [2% deoxycholate detergent (DOC), 0.02 M Tris-HCl, pH 8.8] as outlined in Ref. 21. The

lysates were transferred to eppendorf tubes, and the ECM was isolated in the pellet fraction by centrifugation. The pellets were solubilized by dissolving them in 25 μL of 1% SDS (Fisher Scientific) in 25 mM Tris-HCl, pH 8. The total protein concentration in the DOC soluble fraction was determined through a bicinchoninic acid assay (BCA, Pierce, Rockford, IL). FN in the DOC insoluble fraction was analyzed by electrophoresis and then immunoblotting with R184 antibodies. The amount of DOC insoluble material resolved was normalized to total protein concentration in the DOC soluble fraction before electrophoresis.

DOC insoluble material was electrophoresed in a 7% polyacrylamide gel and then transferred to Hybond ECL nitrocellulose membrane (GE Healthcare). The membrane was incubated with polyclonal R184 antibodies at a dilution of 1:1,000 and then with the secondary goat anti-rabbit IgG (H+L), horseradish peroxidase conjugate antibodies (Invitrogen) at a dilution of 1:5,000. The chemiluminescent 250 kDa FN bands were imaged and quantified through a Chemidoc XRS imaging system (Biorad, Hercules, CA) and Quantity One software (Biorad), respectively. A 25 ng amount of rat plasma FN was used as a positive control in the immunoblots. Rat plasma FN was purified by gelatin-affinity chromatography of rat plasma (Lampire Biologicals, Ottsville, PA). The quantity of FN in each sample was obtained by integrating areas under the peaks defining each band in the immunoblot. The dynamic range of the Chemidoc XRS imaging system is four orders of magnitude, which corresponds to a pixel density of 65,535. To ensure that the readings obtained were in the linear range and not saturated, a number of approaches were used. First, a regression curve with purified rat plasma FN at concentrations ranging between 0 and 200 ng was used to confirm the linear range. Second, inbuilt software was used to highlight bands that were saturated. Finally, imaging was done at different exposure times.

Microscopy and image analysis

Before each incubation period, bright field images of the cells at 10× and 20× magnification were collected using a Carl Zeiss Axiovert 40CL microscope coupled to an Axiocam ICM (Zeiss, Thornwood, New York). Fluorescent images of NIH3T3 cells were obtained as part of the adhesion assay. Two spectrally different filter sets were used to resolve the Hoechst stained nuclei and fluorescein-phalloidin stained actin filaments when assaying for cell adhesion and spreading, respectively. Digital images were recorded by Axiovision software (Zeiss). The images were quantified using Image J software from the National Institutes of Health. Cell number was determined by thresholding Hoechst stained images and using the automated counter to count the cell nuclei. Outlines of the cell nuclei were matched to the numbered nuclei to minimize overlap error. Cell area was determined by thresholding images of fluorescein stained actin filaments and using inbuilt macros in Image J to evaluate highlighted stained areas. Immunostained FN fibrils were imaged using the fluorescein filter. Care was taken to keep imaging exposure times and thresholding parameters constant during microscopy and analysis so as to ensure that different treatments were imaged and analyzed in the same manner.

Statistical analysis

Scatter plots of the experimental data were used to visualize the relationship between biological responses and the concentration of $III_{1\text{-}2}$ and $III_{9\text{-}10}$. Based on this exploratory analysis, linear models were specified and fit using appropriate scaling on both responses and predictors. The significance and the coefficients in the linear models were determined by analysis of variance (ANOVA) and *t*-tests. A two-sided significance level of 5% for was used for *t*-tests, and a 95% confidence interval was used for the mean of the biological responses.

Results

Surface characterization

We recently reported on a strategy for derivatizing polyurethane surfaces with FN domains $III_{1\text{-}2}$ and $III_{9\text{-}10}$.[15] In the study by Chiang et al., we demonstrated that GST-$III_{1\text{-}2}$ and GST-$III_{9\text{-}10}$ had similar binding affinity for activated polyurethane surfaces and that activated polyurethane surfaces were saturated with these domains at a solution concentration of 1 μM. We have used a similar approach to derivatize polyurethane with mixtures of GST-$III_{1\text{-}2}$ and GST-$III_{9\text{-}10}$ (Figure 1A). We first verified the efficacy of coupling by monitoring the contact angles of modified surfaces. The contact angles for surfaces 1, 2, and 5 in Figure 1A were 64°–68°, 48°–54°, and 80°–90°, respectively. We then varied the concentration of GST-$III_{1\text{-}2}$ and GST-$III_{9\text{-}10}$ in solution (**6a** and **6b** in Figure 1A) and used ELISAs to detect FN domains on the surface. The broken line in Figure 1B represents a best fit for $III_{1\text{-}2}$ and $III_{9\text{-}10}$ ELISA absorbance data. GST-$III_{1\text{-}2}$ and GST-$III_{9\text{-}10}$ are saturated on activated polyurethane surfaces at a solution concentration of 1 μM or 50 μg/mL.

To determine that surface saturation of GST-$III_{1\text{-}2}$ and GST-$III_{9\text{-}10}$ at 1 μM is the limiting factor and not saturation of the antibodies on the surface, we conducted a control binding study with FN. The concentration of GST-$III_{9\text{-}10}$ and FN in solution was varied and proteins bound to activated polyurethane surfaces were detected via ELISA. Figure 1C shows results obtained with monoclonal antibodies that bind $III_{9\text{-}10}$ and FN. FN was saturated on the surface at solution concentrations of 0.1 μM or 50 μg/mL. FN has a molecular weight ~10 times higher than the molecular weight of GST-$III_{9\text{-}10}$, and therefore, the experimental molar solution concentration at surface saturation is in agreement with the expected value of one tenth the solution concentration of GST-$III_{9\text{-}10}$ at surface saturation. This finding with GST-$III_{9\text{-}10}$ can be extended to GST-$III_{1\text{-}2}$ because both proteins are comparable in structure and in molecular weight. Moreover, we had previously shown, through competitive binding assays with mixtures of GST-$III_{1\text{-}2}$ and GST-$III_{9\text{-}10}$, that these two molecules exhibit similar binding characteristics for activated polyurethane surfaces.[15] Therefore, the experimental design space for our studies was defined by the concentration limits of GST-$III_{1\text{-}2}$ and GST-$III_{9\text{-}10}$ for surface saturation and had an upper bound of 1 μM or 50 μg/mL and a lower bound of zero.

Relationships between the composition of $III_{1\text{-}2}$ and $III_{9\text{-}10}$ and the amount of FN in the ECM

We had previously demonstrated that cells cultured on surfaces with a one to one ratio of $III_{1\text{-}2}$ and $III_{9\text{-}10}$ had higher extracellular staining of FN than cells cultured on $III_{9\text{-}10}$ surfaces alone.[15] We examined the effect of varying GST-$III_{1\text{-}2}$ and GST-$III_{9\text{-}10}$ on the amount of fibrillar FN formed by NIH 3T3 fibroblasts. Immunoblotting of FN in the DOC insoluble fraction of cell lysates is the standard

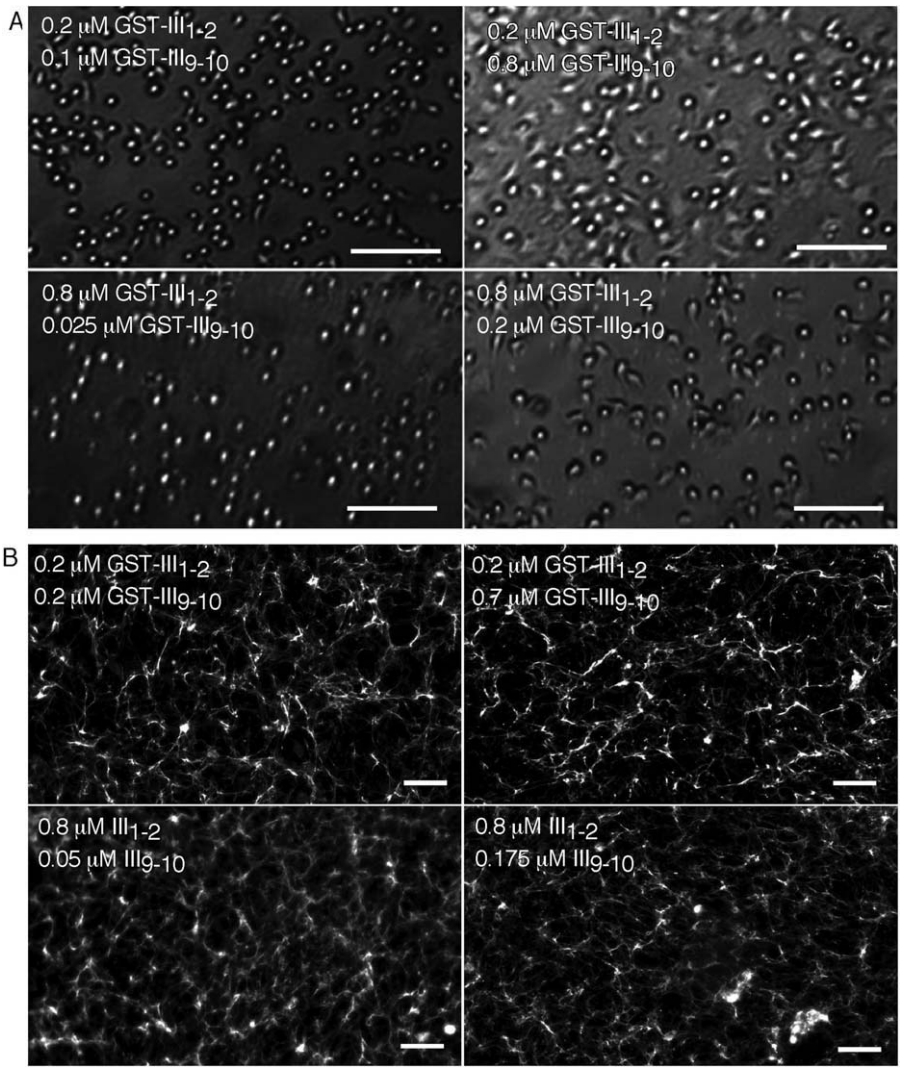

Figure 2. Microscopy of cells and extracellular FN on derivatized surfaces.

Surface chemistry was varied by keeping GST-III$_{1\text{-}2}$ fixed at 0.2 μM and 0.8 μM and changing GST-III$_{9\text{-}10}$ from 0.1 to 0.8 μM and 0.025 to 0.2 μM, respectively. NIH3T3 fibroblasts were cultured for half an hour in serum free media then 24 h at 37°C in FN depleted serum on derivatized surfaces. A: Bright field 10× images of cells on surfaces after half an hour cell culture and a change of media. Scale bar = 100 μm. B: Immunofluorescence images of extracellular FN fibrils after the 24-h culture period. Scale bar = 20 μm.

assay for measuring the amount of fibrillar FN associated with cells.[7] In the first approach, we examined the effect of fixing GST-III$_{1\text{-}2}$ and varying GST-III$_{9\text{-}10}$ on the amount of FN fibrils formed. We chose two concentrations of GST-III$_{1\text{-}2}$: a high concentration corresponding to 0.8 μM and a low concentration corresponding to 0.2 μM. The concentration of GST-III$_{9\text{-}10}$ was varied at seven equally spaced intervals from 0.1 to 0.8 μM when GST-III$_{1\text{-}2}$ was 0.2 μM and from 0.025 to 0.2 μM when GST-III$_{1\text{-}2}$ was 0.8 μM. Varying GST-III$_{9\text{-}10}$ is more informative than varying GST-III$_{1\text{-}2}$ as we had previously established that cells did not adhere to surfaces with GST-III$_{1\text{-}2}$.[15] We had also shown that the highly hydrophobic carbonate terminated surface (Surface 5, in Figure 1A) has reduced cell attachment compared with a protein saturated surface when similar amounts of GST-III$_{9\text{-}10}$ are present.[15] Therefore, it was essential to have a background to the bound GST-III$_{1\text{-}2}$ and GST-III$_{9\text{-}10}$ that was protein-like. Individual GST molecules provided this background when total concentration of GST-III$_{1\text{-}2}$ and GST-III$_{9\text{-}10}$ was less than the saturation limit of 50 μg/mL.

Conditions that favor cell spreading activate mechanisms involved in FN fibrillogenesis.[22,23] After half an hour in serum free culture media, the media was changed to media with FN depleted serum and images were taken soon after so as to visualize cell spreading on functionalized surfaces (Figure 2A). There were clear morphological differences in cell shape on the different treatments. At constant, GST-III$_{1\text{-}2}$ increasing GST-III$_{9\text{-}10}$ resulted in better cell spreading (Figure 2A). This was observed on surfaces with low and high GST-III$_{1\text{-}2}$ concentrations (0.2 and 0.8 μM). We did not visually detect a difference in cell numbers at constant GST-III$_{1\text{-}2}$ and varying GST-III$_{9\text{-}10}$ concentrations. However, there were fewer cells on surfaces with a GST-III$_{1\text{-}2}$ concentration of 0.8 μM than there were on surfaces with a GST-III$_{1\text{-}2}$ concentration of 0.2 μM (Figure 2A). After a 24-h culture period, the cells were fixed and immunostained for extracellular FN (Figure 2B). At low GST-III$_{1\text{-}2}$, FN fibril density was lower than at high GST-III$_{1\text{-}2}$ concentration but staining intensity was higher at low GST-III$_{1\text{-}2}$ concentration. We could not visually discern any differences in fibrillar FN

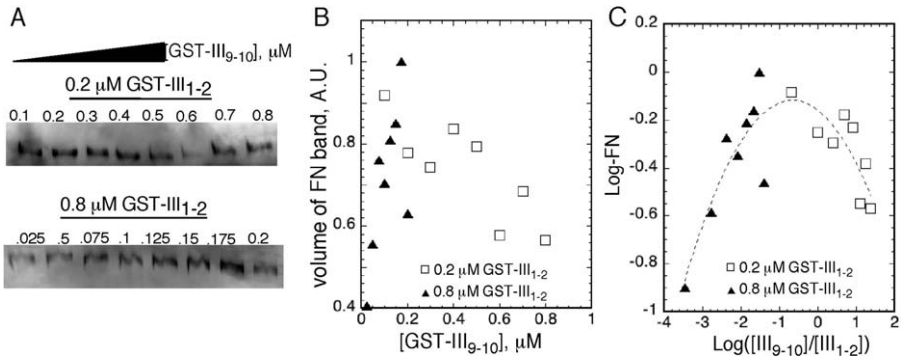

Figure 3. The amount of FN in the ECM is dependent on the ratio of $III_{9\text{-}10}$ to $III_{1\text{-}2}$.

Surface chemistry was varied by keeping the concentration of GST-$III_{1\text{-}2}$ or [$III_{1\text{-}2}$] fixed at 0.2 μM and 0.8 μM and changing GST-$III_{9\text{-}10}$ concentration or [$III_{9\text{-}10}$] from 0.1 to 0.8 μM and 0.025 to 0.2 μM, respectively. NIH3T3 fibroblasts were cultured for half an hour in serum free media then 24 h at 37°C in FN depleted serum on derivatized surfaces. Fibrillar FN was then isolated in DOC insoluble cell extracts, electrophoresed and immunoblotted. The amount electrophoresed in the different treatments was matched to total protein concentration in the DOC soluble fraction. A: Immunoblot of FN with R184 antibodies after SDS-PAGE. The bands correspond to the 250 kDa band of reduced FN. B: Image analysis of the volume of FN band vs. [$III_{9\text{-}10}$]. The *y*-axis in the figure represents the volume of each band divided with 5×10^7 (the volume of 25 ng of rat plasma FN control). C: The logarithm of the volume of the FN band, Log-FN vs. Log([$III_{9\text{-}10}$]/[$III_{1\text{-}2}$]). The broken line is a quadratic fit to the experimental data.

structure between samples treated with different amounts of GST-$III_{9\text{-}10}$ and the same amount of GST-$III_{1\text{-}2}$.

We measured the amount of fibrillar FN in the ECM of cells cultured on the functionalized surfaces for 24 h. This is present in DOC insoluble extracts of cell monolayers. DOC insoluble material was extracted from cells cultured on the derivatized polyurethane surfaces and immunoblotted for FN. Figure 3A shows a FN immunoblot of extracted fibrillar FN. The amount electrophoresed was normalized to cell count before the samples were loaded onto a polyacrylamide gel. This was done by using the total protein concentration from BCA assays of the DOC soluble fraction. The DOC soluble fraction contains lysed cells, and therefore, the thickness of each band in the immunoblot in Figure 3A is an indicator of the amount of fibrillar FN per cell. Figure 3A shows the relationship between the amount of fibrillar FN with changing GST-$III_{9\text{-}10}$. At the low concentrations of GST-$III_{1\text{-}2}$ (0.2 μM), increasing GST-$III_{9\text{-}10}$ from 0.1 to 0.8 μM decreases the amount of fibrillar FN. On the other hand, at high concentrations of GST-$III_{1\text{-}2}$ (0.8 μM), increasing GST-$III_{9\text{-}10}$ from 0.025 μM to 0.2 μM increases the amount of fibrillar FN. These changes were quantified by image analysis software (Figure 3B). Figure 3B shows a reversal in the relationship between FN fibril amount and the amount of GST-$III_{9\text{-}10}$ from low to high GST-$III_{1\text{-}2}$. FN fibril formation does not correlate with cell spreading because cell spreading increases with increasing $III_{9\text{-}10}$ concentration at both low and high $III_{1\text{-}2}$ concentrations (Figures 2A and 3B). The relationship between the amount of fibrillar FN and $III_{1\text{-}2}$ and $III_{9\text{-}10}$ composition suggested that FN fibril amount was dependent on the ratio between $III_{9\text{-}10}$ and $III_{1\text{-}2}$.

We examined the relationship between the logarithm of the amount of fibrillar FN and the logarithm of the ratio of concentrations of $III_{9\text{-}10}$ to $III_{1\text{-}2}$ in GST tagged $III_{1\text{-}2}$ and $III_{9\text{-}10}$ mixtures (Log([$III_{9\text{-}10}$]/[$III_{1\text{-}2}$]). The logarithm transformation helps with scaling and provides a way of visualizing possible relationships. Figure 3C shows the logarithm of FN fibril amount vs. Log([$III_{9\text{-}10}$]/[$III_{1\text{-}2}$]). The data in Figure 3C suggests a quadratic relationship between logarithm of the response (amount of fibrillar FN) and Log([$III_{9\text{-}10}$]/[$III_{1\text{-}2}$]). We examined this possibility through a regression analysis of the standardized response:

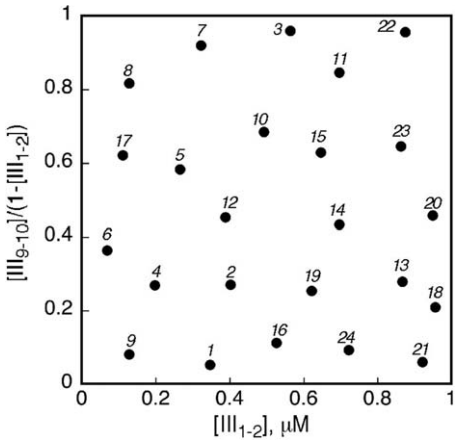

Figure 4. A scatter plot of $III_{1\text{-}2}$ and $III_{9\text{-}10}$ concentrations used to optimally sample the design space.

The design space is defined by a unit square with dimensions defined by $0 < [III_{1\text{-}2}] < 1$ μM and $0 < [III_{9\text{-}10}]/(1 - [III_{1\text{-}2}]) < 1$. The *y*-axis represents scaled $[III_{9\text{-}10}] = ([III_{9\text{-}10}]/(1 - [III_{1\text{-}2}]))$ and each point represents a mixture composition.

$$y_T = (y - y_m)/\sigma_y \quad (1)$$

In Eq. 1, *y* is the logarithm of the amount of fibrillar FN (Log-FN), y_T and y_m are the standardized Log-FN and mean Log-FN, respectively, and σ_y is the standard deviation of *y*. Standardization helps in comparing data from different experiments. Figure 3C suggests a linear fit would be inappropriate and the data trends toward a quadratic fit. Such a fit with

$$y_T = a + b\mathrm{Log}([III_{9-10}]/[III_{1-2}]) + c\{\mathrm{Log}([III_{9-10}]/[III_{1-2}])\}^2 \quad (2)$$

results in estimates for *a*, *b*, and *c* of 0.82 (*P*-value of 0.00), −0.55 (*P*-value of 0.00), and −0.42 (*P*-value of 0.00), respectively, and an R^2 value of 0.67. This fit is represented by the dotted line in Figure 3C. Thus, the standardized logarithm of the amount of fibrillar FN, y_T, fits a quadratic relationship

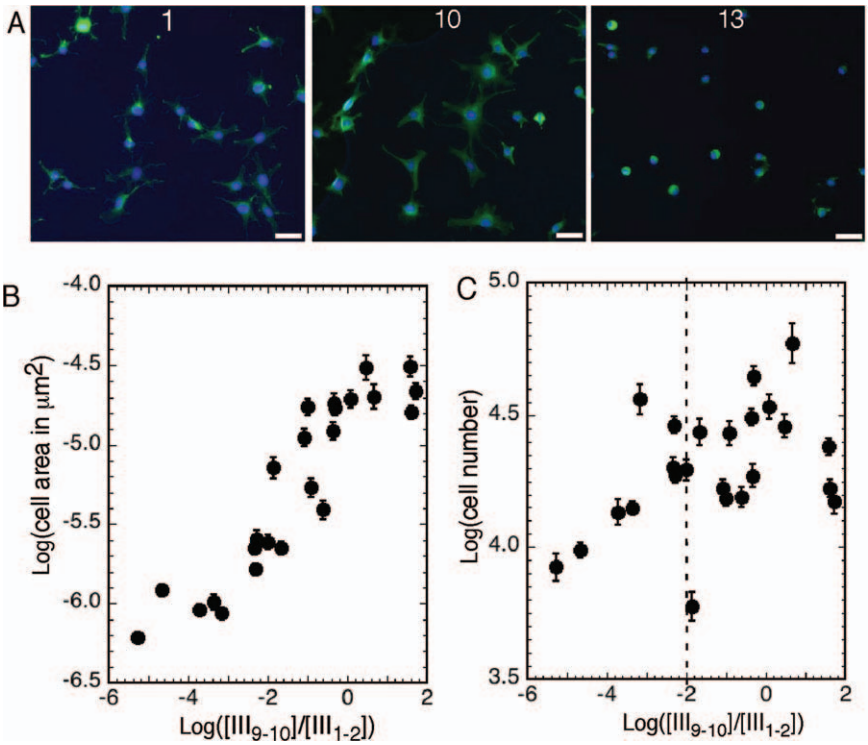

Figure 5. Varying the ratio of III_{1-2} and III_{9-10} influences cell spreading.

Cell adhesion and spreading on surfaces treated with the coverage design in Figure 4. A: Immunofluorescence images of NIH3T3 fibroblasts after an hour culture in serum free media. The blue and green colors correspond to Hoeschst stained nuclei and actin stained by fluorescein-phalloidin, respectively. The numbers represent the solution concentrations in Figure 4. Scale bar = 20 μm. Logarithm of cell area (B) and cell number (C) vs. Log($[III_{9-10}]/[III_{1-2}]$). Error bars in (B) and (C) represent a 95% confidence interval of 47–109 cells per treatment and 16 fields per treatment, respectively.

with the logarithm of the ratio between III_{9-10} and III_{1-2} and has a maximum when Log($[III_{9-10}]/[III_{1-2}]$) is equal to -0.65 or $[III_{9-10}]/[III_{1-2}]$ is equal to 0.52. A 95% confidence interval for the peak value of $[III_{9-10}]/[III_{1-2}]$ is (0.30, 0.90). The *F*-statistics on a lack of fit for the model yields a *P*-value of 0.00. We can, therefore, conclude that the quadratic model is a significant fit. These results demonstrate that III_{1-2} influences the relationship between FN fibril amount and III_{9-10} and this relationship is sensitive to the ratio between III_{9-10} and III_{1-2}. Because the ratio of III_{9-10} to III_{1-2} is important for FN fibril amount, we examined the influence of the ratio of III_{9-10} to III_{1-2} on FN fibril amount, and the cellular responses of adhesion and spreading in the entire design space.

Optimal sampling of surface amounts of III_{1-2} and III_{9-10} using a coverage design

A coverage design was used to optimally sample the entire design space. The concentration of III_{1-2} in the design space has a range between zero and 1 μM and the range of III_{9-10} in a mixture with III_{1-2} is between zero and 1-$[III_{1-2}]$ μM. Therefore, the design space covers the concentration of III_{1-2} ranging from 0 to 1 μM and a scaled concentration of III_{9-10} ranging from zero to one where

$$\text{scaled}[III_{9-10}] = [III_{9-10}]/(1 - [III_{1-2}]) \qquad (3)$$

From a candidate set of 100 × 100 equally spaced points on a unit square representing the design space, we used statistical software to select a subset of 24 points which best covered the design space. Figure 4 shows the 24 mixture compositions represented by the scaled III_{9-10} concentration vs. III_{1-2} concentration. Figure 4 demonstrates that these compositions uniformly cover the design space. It is important to note that the concentrations of the FN domains are the concentrations of the GST tagged FN domains. Therefore, each point in Figure 4 corresponds to surface saturation and total molar concentration of GST-III_{1-2} and GST-III_{9-10} of 1 μM. We had previously determined that the ratio of III_{1-2} and III_{9-10} influences FN fibrillar formation (Figure 3C). Figure 4 varies the ratio of the two domains but, unlike Figure 3C, keeps the total amount of the affinity tag GST and the FN domains constant. Thus, the experimental design reduces the system to two variables: the ratio of III_{9-10} to III_{1-2} ($[III_{9-10}]/[III_{1-2}]$) and a cellular response.

Cell adhesion, cell spreading, and FN fibril formation on surfaces treated with a coverage design

The cellular responses to activated polyurethane surfaces treated with the coverage design were then determined. Cell adhesion and spreading were evaluated through image analysis of fluorescence micrographs of NIH3T3 fibroblasts cultured for 1 h in media without serum (Figure 5A). The adhesion and spreading assays were done at lower cell densities than those used for FN fibril formation so that individual cells could be identified and analyzed. A quantitative analysis of cell spreading is shown in Figure 5B. It demonstrates that cell spreading increases with increasing ratio of III_{9-10} to III_{1-2}. This is in line with earlier observations that at constant III_{1-2}, increasing III_{9-10} resulted in better cell spreading (Figure 2A). The relationship between cell adhesion and the ratio of III_{9-10} to III_{1-2} is less well defined

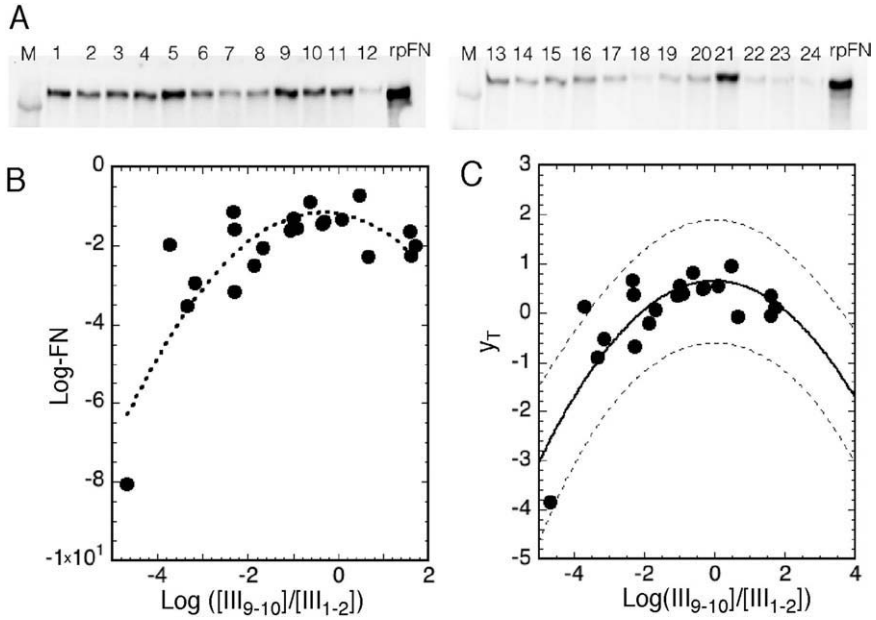

Figure 6. FN fibril formation is optimized when the ratio of the amount of $III_{9\text{-}10}$ to $III_{1\text{-}2}$ is equal to one.

NIH3T3 fibroblasts were cultured for 24 h at 37°C in FN depleted serum on derivatized surfaces treated $III_{1\text{-}2}$ and $III_{9\text{-}10}$ mixtures generated by the coverage design. The amount of FN in the ECM was measured by immunoblotting DOC insoluble extracts. The amount DOC extract analyzed was normalized to total protein concentration before loading the samples for electrophoresis. A: FN immunoblot after treatment with R184 antibodies. The numbers 1–24 represent the surface coverage concentrations in Figure 4. *M* and *rpFN* are 250 kDa marker and 25 ng of rat plasma FN loading control. The logarithm (B) and transformed logarithm (C) of the amount of fibrillar FN vs. Log($[III_{9\text{-}10}]/[III_{1\text{-}2}]$ has a quadratic fit. The broken lines in (C) represent a 95% confidence interval for the quadratic fit (solid line) of the experimental data.

(Figure 5C). When the ratio of the cell-binding domain to the FN binding domain is less than 0.14, or Log($[III_{9\text{-}10}]/[III_{1\text{-}2}]$) is less than −2, the number of adherent cells increases with increasing ratio of $III_{9\text{-}10}$ to $III_{1\text{-}2}$. There is no discernable relationship between cell adhesion and Log($[III_{9\text{-}10}]/[III_{1\text{-}2}]$) when Log($[III_{9\text{-}10}]/[III_{1\text{-}2}]$) is greater than −2 due to a large variation in cell numbers. These variations in cell adhesion at higher ratios of $III_{9\text{-}10}$ to $III_{1\text{-}2}$ may be due to other unaccountable factors that influence cell adhesion. Nonetheless, experimental results indicate that cell spreading on derivatized surfaces increases with the ratio of $III_{9\text{-}10}$ to $III_{1\text{-}2}$.

The effect of varying the ratio of $III_{1\text{-}2}$ and $III_{9\text{-}10}$ on the amount of FN in the ECM of NIH3T3 fibroblasts was determined by immunoblotting DOC insoluble cell extracts. To account for bias due to differences in cell numbers, the amount of DOC insoluble extracts electrophoresed from different treatments was matched to total protein concentration in the DOC soluble fraction. For each of the 24 mixture compositions defined by the coverage design in Figure 4, the amount of DOC insoluble FN or fibrillar FN was quantified as the intensity of the 250 kDa FN band divided by the intensity of the 25 ng rat plasma FN band (Figure 6A). Scatter plots of the amount of fibrillar FN vs. the logarithm of the ratio of $III_{9\text{-}10}$ to $III_{1\text{-}2}$ in GST-tagged mixtures of the domains, Log($[III_{9\text{-}10}]/[III_{1\text{-}2}]$), are presented in Figures 6B,C. Figure 6B shows that the amount of FN in the ECM is dependent on the ratio of $III_{9\text{-}10}$ and $III_{1\text{-}2}$. Fibrillar FN increases with the ratio of $III_{9\text{-}10}$ to $III_{1\text{-}2}$ to a maximum value and then decreases with increasing ratio of $III_{9\text{-}10}$ to $III_{1\text{-}2}$.

We examined whether the amount of fibrillar FN in the ECM of cells cultured on surfaces treated with the coverage design, could be fit to a quadratic relationship. The data in Figure 6B was first standardized using Eq. 1 and then fit to the quadratic in Eq. 2. The coefficients *a*, *b*, and *c* for a quadratic fit of the transformed response, y_T, are 0.64 (*P*-value of 0.00), −0.12 (*P*-value of 0.31), and −0.71 (*P*-value of 0.00), respectively. The R^2 value for this fit is 0.67, and the *F*-test for lack of fit yields a *P*-value of 0.00 indicating the model is significant. The coefficient for *b* is not significant as it has a *P*-value that is greater than 0.05, and therefore, the hypothesis that *b* is zero should not be rejected. Refitting the quadratic model (Eq. 2) without the coefficient *b* gives

$$y_T = a + c\{\mathrm{Log}[III_{9-10}]/[III_{1-2}]\}^2 \quad (4)$$

The result of this fit is a curve whose maximum occurs at zero. The experimental data in Figures 6B,C visually agree with this model as the maximum amount of FN fibrils occurs when the concentrations of $III_{1\text{-}2}$ and $III_{9\text{-}10}$ are equal. Fitting Eq. 4 yields estimates for *a* and *c* of 0.64 (*P*-value of 0.00) and −0.15 (*P*-value of 0.00), respectively. The R^2 value of this relationship is 0.67 and the *F*-statistic has a *P*-value of 0.00 indicating a significant fit. Figure 6C shows the model fit (solid black line) and a 95% confidence interval (broken lines). The amount of fibrillar FN is dependent on the ratio of $III_{9\text{-}10}$ to $III_{1\text{-}2}$ and has a maximum when the two domains are equal.

Cell density through cell–cell contacts influences a variety of cell responses including the amount of FN in the ECM.[24,25] We examined if there was a correlation between cell number and the amount of fibrillar FN. The total protein concentration in the soluble DOC fraction was used to normalize the DOC insoluble extracts from different treatments before electrophoresis in the studies in Figures 3 and 6. It contains intracellular proteins and is a measure of cell number at longer culture periods. A plot of logarithm of total

protein concentration derived from the DOC supernatants of cells cultured on the coverage design for 24 h vs. the ratio of III_{9-10} to III_{1-2} is shown in Supporting Information Figure 1. If the lowest protein concentration is excluded, the remaining points have random scatter and there is no discernable relationship between protein concentration and logarithm of the ratio of III_{9-10} to III_{1-2}. Moreover, a plot of the logarithm amount of fibrillar FN vs. the logarithm of total protein concentration (Supporting Information Figure 1B) shows no correlation between the two variables. Cell density does not introduce bias into the amount of fibrillar FN in our experiments.

Two different experimental designs show that the surface ratio of III_{9-10} to III_{1-2} influences the amount of fibrillar FN. This has a peak value at a specific ratio of the two domains. The coverage design which samples optimally in the design space shows that the maximum in the amount of FN fibrils formed occurs when equal amounts of III_{1-2} and III_{9-10} are present on a surface. Cell spreading increases with increasing ratio of III_{9-10} to III_{1-2}. Cell spreading and the amount of fibrillar FN can be directed on synthetic scaffolds by varying the ratio of III_{1-2} and III_{9-10} on the surface.

Discussion

The goal of ours study was to determine if the amount of fibrillar FN assembled by cells could be synthetically manipulated by varying the amount of FN and cell binding domains, III_{1-2} and III_{9-10}, immobilized on a surface. We had previously reported on a surface chemistry strategy that robustly immobilized these domains on polyurethane surfaces. We used the same surface chemistry approach to investigate the effect of different amounts of III_{1-2} and III_{9-10} on the amount of fibrillar FN, as well as to explore any correlations between fibrillar FN amount, cell adhesion and cell spreading. We used two experimental designs for these studies. In the first design, we fixed III_{1-2} and varied III_{9-10}. In the second strategy, we kept the solution concentration constant and varied the amounts of III_{1-2} and III_{9-10}. In the latter strategy, we used a coverage design to obtain as wide a range of mixture concentrations as possible. In both experimental designs, the amount of fibrillar FN was dependent on the ratio of III_{9-10} to III_{1-2} and had a peak value of one for the coverage design. There was no correlation between cell spreading, cell adhesion, and the amount of FN in the ECM on surfaces derivatized with FN domains. Cell spreading increased with increasing ratio of III_{9-10} to III_{1-2}. At short time periods, cell adhesion increased with increasing ratio of III_{9-10} to III_{1-2} for low ratios of III_{9-10} to III_{1-2} but plateaued at high ratios of III_{9-10} to III_{1-2} (III_{9-10} roughly equal to seven times III_{1-2}). At these high III_{9-10} to III_{1-2} ratios, a mathematical relationship between cell adhesion and surface composition could not be established graphically due to the large variation in cell numbers. There may be other factors at play in cell adhesion at high ratios of III_{9-10} to III_{1-2}. At longer time periods, there was no relationship between cell adhesion and FN fibril amount.

One question that arises from this study is how surfaces derivatized with III_{1-2} and III_{9-10} advance existing models of the assembly of FN into fibrils. The challenge therein lies in the fact that these models have been developed using full-length FN, recombinant FN with one or more domains deleted or soluble protein fragments,[7] whereas our studies were carried out with immobilized FN domains. As such, the prevailing model of FN fibrillar assembly, which is dependent on cell-mediated extension of full-length FN, does not fit our surfaces which are conjugated with disconnected domains. Moreover, the cell-mediated extension model of FN suggests a link between cell spreading, cell adhesion, and the amount of FN in the ECM but we observed no correlation between cell spreading and the amount of fibrillar FN on III_{1-2} and III_{9-10} derivatized surfaces. The link between cell-spreading and FN fibril formation is dynamic,[10] and our studies, which are based on end-point responses, may fail to capture these time dependent responses. The work by Xu et al.[26] has parallels with our work with respect to the effect of mixing FN and cell binding domains. They show synergy between III_1 and a fragment encompassing III_{9-10} in mediating the formation of FN fibrils in FN null fibroblasts.[26] These cells cannot produce FN but can assemble it into fibrils if FN is provided in the media. They also show that FN null fibroblasts do not assemble a FN matrix on surfaces treated with III_{9-10} alone. This finding is in agreement with our observations because at high ratios of III_{9-10} to III_{1-2} we found low amounts of fibrillar FN and the maximum amount of FN occurred when III_{1-2} and III_{9-10} were present in equal amounts. The work by Xu et al. also suggests that FN domains required for optimal assembly of FN into an ECM may be different from FN domains needed for optimal cell adhesion or spreading. We show that the relationship between cell spreading and surface mixtures of III_{1-2} and III_{9-10} is distinct to that of FN fibrillar formation on similarly treated surfaces. Xu et al. suggest that an unknown receptor may bind III_1 and activate events associated with FN fibril formation. Although this is a possibility, our findings favor a molecular mechanism of FN fibril formation that is sensitive to the ratio of immobilized III_{1-2} and III_{9-10}.

In a previous study, we proposed that on a surface with equal amounts of the FN binding and the cell-binding domain, III_{1-2} may sequester FN secreted by cells.[15] Thus, one III_{1-2} molecule may bind a number of FN molecules and provide for clustering of FN. The importance of clustering in activating signaling pathways inside the cells has long been established.[27–30] Clustering brings molecules in close proximity and increases the probability of binding events between binding partners. Moreover, FN clustering has been shown to precede actin mediated unfolding of FN molecules.[31] Cell attachment and spreading on the other hand are wholly dependent on III_{9-10} concentration and cells do not attach to III_{1-2}.[15] Varying the ratio of III_{1-2} to III_{9-10} may lead to differences in the cluster size and spacing of full-length FN bound to III_{1-2}. FN-III_{1-2} clusters may enhance early events that initialize the formation of FN fibrils on surfaces derivatized with both III_{1-2} and III_{9-10}. This clustering mechanism may explain the different trends in the responses of FN fibril amount and cell spreading with varying amounts of III_{1-2} and III_{9-10}.

We demonstrate that by varying the ratio and quantities of III_{1-2} and III_{9-10} on a surface one can directly impact the amount of FN in the ECM of fibroblasts. This has relevance in the design of wound dressing materials in chronic wounds. A synthetic material with immobilized III_{1-2} and III_{9-10} may be used as a synthetic ECM to selectively enhance FN fibril formation and subsequently tissue repair in a chronic wound bed. Unlike decellularized ECMs, this alternative approach provides an element of control of biological responses involved in wound healing. Moreover, the mathematical relationships

obtained from experimental data can be used as a predictive tool in the design of synthetic scaffolds for tissue growth.

Acknowledgments

We are grateful to Dr. Jean E. Schwarzbauer for the gift of antibodies and bacteria encoding for III_{1-2} and III_{9-10} and to Dr. Jeffrey E. Schwartz for the gift of phosphonic acid.

Literature Cited

1. Hedman K, Kurkinen M, Alitalo K, Vaheri A, Johansson S, Hook M. Isolation of the pericellular matrix of human fibroblast cultures. *J Cell Biol*. 1979;81:83–91.
2. Hedman K, Johansson S, Vartio T, Kjellen L, Vaheri A, Hook M. Structure of the pericellular matrix: association of heparan and chondroitin sulfates with fibronectin-procollagen fibers. *Cell*. 1982;28:663–671.
3. Yates CC, Bodnar R, Wells A. Matrix control of scarring. *Cell Mol Life Sci*. 2011;68:1871–1881.
4. Wysocki AB, Grinnell F. Fibronectin profiles in normal and chronic wound fluid. *LabInvest*. 1990;63:825–831.
5. Herrick SE, Ireland GW, Simon D, McCollum CN, Ferguson MW. Venous ulcer fibroblasts compared with normal fibroblasts show differences in collagen but not fibronectin production under both normal and hypoxic conditions. *J Invest Dermatol*. 1996;106:187–193.
6. Agren MS, Werthen M. The extracellular matrix in wound healing: a closer look at therapeutics for chronic wounds. *Int J Low Extrem Wounds*. 2007;6:82–97.
7. Singh P, Carraher C, Schwarzbauer JE. Assembly of fibronectin extracellular matrix. *Annu Rev Cell Dev Biol*. 2010;26:397–419.
8. McDonald JA, Quade BJ, Broekelmann TJ, LaChance R, Forsman K, Hasegawa E, Akiyama S. Fibronectin's cell-adhesive domain and an amino-terminal matrix assembly domain participate in its assembly into fibroblast pericellular matrix. *J Biol Chem*. 1987;262:2957–2967.
9. Sechler JL, Rao H, Cumiskey AM, Vega-Colon I, Smith MS, Murata T, Schwarzbauer JE. A novel fibronectin binding site required for fibronectin fibril growth during matrix assembly. *J Cell Biol*. 2001;154:1081–1088.
10. Ohashi T, Kiehart DP, Erickson HP. Dynamics and elasticity of the fibronectin matrix in living cell culture visualized by fibronectin-green fluorescent protein. *Proc Natl Acad Sci USA*. 1999;96:2153–2158.
11. Aguirre KM, McCormick R, Schwarzbauer JE. Fibronectin self-association is mediated by complementary sites within the amino-terminal one-third of the molecule. *J Biol Chem*. 1994; 269:27863–27868.
12. Hocking DC, Sottile J, McKeown-Longo PJ. Fibronectin's III-1 module contains a conformation-dependent binding site for the amino-terminal region of fibronectin. *J Biol Chem*. 1994;269: 19183–19187.
13. Hocking DC, Kowalski K. A cryptic fragment from fibronectin's III1 module localizes to lipid rafts and stimulates cell growth and contractility. *J Cell Biol*. 2002;158:175–184.
14. Chernousov MA, Fogerty FJ, Koteliansky VE, Mosher DF. Role of the I-9 and III-1 modules of fibronectin in formation of an extracellular fibronectin matrix. *J Biol Chem*. 1991;266:10851–10858.
15. Chiang C, Karuri SW, Kshatriya PP, Schwartz J, Schwarzbauer J, Karuri NW. A surface derivatization strategy for combinatorial analysis of cell response to mixtures of protein domains. *Langmuir*. 2011;28:548–556.
16. Abraham M. Equilibrium contact angles: theory and measurement. *Colloids Surf A*. 1996;116:55–61.
17. Karuri NW, Lin Z, Rye HS, Schwarzbauer JE. Probing the conformation of the fibronectin III1–2 domain by fluorescence resonance energy transfer. *J Biol Chem*. 2009;284:3445–3452.
18. Royle JA, Nychka D. An algorithm for the construction of spatial coverage designs with implementation in SPLUS. *Comput Geosci*. 1998;24:479–488.
19. Lam RLH, Welch WJ, Young SS. Uniform coverage designs for molecule selection. *Technometrics*. 2002;44:99–109.
20. Furrer R, Nychka D, Sain S. R Package Fields, Version 6.3. Available at: http://www.image.ucar.edu/Software/Fields.
21. Midwood KS, Wierzbicka-Patynowski I, Schwarzbauer JE. Preparation and analysis of synthetic multicomponent extracellular matrix. *Methods Cell Biol*. 2002;69:145–161.
22. Green JA, Berrier AL, Pankov R, Yamada KM. Beta1 integrin cytoplasmic domain residues selectively modulate fibronectin matrix assembly and cell spreading through talin and Akt-1. *J Biol Chem*. 2009;284:8148–8159.
23. Lemmon CA, Chen CS, Romer LH. Cell traction forces direct fibronectin matrix assembly. *Biophys J*. 2009;96:729–738.
24. Wu C, Bauer JS, Juliano RL, McDonald JA. The alpha 5 beta 1 integrin fibronectin receptor, but not the alpha 5 cytoplasmic domain, functions in an early and essential step in fibronectin matrix assembly. *J Biol Chem*. 1993;268:21883–21888.
25. Wierzbicka-Patynowski I, Schwarzbauer JE. The ins and outs of fibronectin matrix assembly. *J Cell Sci*. 2003;116:3269–3276.
26. Xu J, Bae E, Zhang Q, Annis DS, Erickson HP, Mosher DF. Display of cell surface sites for fibronectin assembly is modulated by cell adherence to 1F3 and C-terminal modules of fibronectin. *PLoS One*. 2009;4:1–12.
27. Ali O, Guillou H, Destaing O, Albiges-Rizo C, Block MR, Fourcade B. Cooperativity between integrin activation and mechanical stress leads to integrin clustering. *Biophys J*. 2011;100: 2595–2604.
28. Kornberg L, Earp HS, Parsons JT, Schaller M, Juliano RL. Cell adhesion or integrin clustering increases phosphorylation of a focal adhesion-associated tyrosine kinase. *J Biol Chem*. 1992; 267:23439–23442.
29. Slater JH, Frey W. Nanopatterning of fibronectin and the influence of integrin clustering on endothelial cell spreading and proliferation. *J Biomed Mater Res A*. 2008;87:176–195.
30. Wang W, Zhu J, Springer TA, Luo BH. Tests of integrin transmembrane domain homo-oligomerization during integrin ligand binding and signaling. *J Biol Chem*. 2011;286:1860–1867.
31. Pankov R, Cukierman E, Katz BZ, Matsumoto K, Lin DC, Lin S, Hahn C, Yamada KM. Integrin dynamics and matrix assembly: tensin-dependent translocation of alpha(5)beta(1) integrins promotes early fibronectin fibrillogenesis. *J Cell Biol*. 2000;148: 1075–1090.

Manuscript received Dec. 2, 2011, and revision received Feb. 8, 2012.